Journal of South American Earth Sciences 54 (2014) 71–81

Contents lists available at ScienceDirect

Journal of South American Earth Sciences

journal homepage: www.elsevier.com/locate/jsames

Contrasting Ordovician high- and low-pressure metamorphism related to a microcontinent-arc collision in the Eastern Cordillera of Perú (Tarma province)

Arne P. Willner [a, b, *], Colombo C.G. Tassinari [c], José F. Rodrigues [d], Jorge Acosta [e], Ricardo Castroviejo [f], Miguel Rivera [g]

[a] Institut für Mineralogie und Kristallchemie, Universität Stuttgart, Azenbergstr. 18, 70174 Stuttgart, Germany
[b] Institut für Geologie, Mineralogie und Geophysik, Ruhr-Universität, 44780 Bochum, Germany
[c] Instituto de Geociéncias da Universidade de São Paulo, Rua do Lago 562, CEP 05508-080, Brazil
[d] Faculdade de Engenharia, Universidade de Porto, Rua Dr. Roberto Frias, s/n 4200-465 Porto, Portugal
[e] Instituto Geológico Minero y Metalúrgico, Av. Canadá 1470, San Borja, Lima 41, Perú
[f] Universidad Politécnica de Madrid, Escuela Técnica Superior de Ingenieros de Minas y Energía, c/ Ríos Rosa 21, 28003 Madrid, Spain
[g] Av. Belén 323, dpt.303, Lima 27, San Isidro, Perú

ARTICLE INFO

Article history:
Received 22 January 2014
Accepted 12 May 2014
Available online 24 May 2014

Keywords:
Garnet amphibolite
Sm–Nd mineral isochron
High pressure
Microcontinent-arc collision
PT pseudosection

ABSTRACT

High-pressure conditions of 11–13 kbar/500–540 °C during maximum burial were derived for garnet amphibolite in the Tapo Ultramafic Massif in the Eastern Cordillera of Peru using a PT pseudosection approach. A Sm–Nd mineral-whole rock isochron at 465 ± 24 Ma dates fluid influx at peak temperatures of ~600 °C and the peak of high pressure metamorphism in a rodingite of this ultramafic complex. The Tapo Ultramafic Complex is interpreted as a relic of oceanic crust which was subducted and exhumed in a collision zone along a suture. It was buried under a metamorphic geotherm of 12–13 °C/km during collision of the Paracas microcontinent with an Ordovician arc in the Peruvian Eastern Cordillera. The Ordovician arc is represented by the western Marañon Complex. Here, low PT conditions at 2.4–2.6 kbar, 300–330 °C were estimated for a phyllite–greenschist assemblage representing a contrasting metamorphic geotherm of 32–40 °C/km characteristic for a magmatic arc environment.

1. Introduction

The major characteristics of the Andes are an almost continuous calc-alkaline igneous activity at the Pacific convergent margin throughout Phanerozoic times and the presence of innumerable pre-Mesozoic metamorphic basement areas throughout the entire length of the chain (e.g. Ramos and Aleman, 2000; Ramos, 2008, 2009, 2010). These basement areas represent deep-seated magmatic arcs, accretionary prisms and collision zones of microplates, where crustal growth, substantial crustal thickening and erosion occurred. Allochthonous microcontinents were recognized in the past decades as summarized by Ramos (2009). In many cases microcontinents were defined by the presence of suture zones that contain chains of disrupted ophiolitic bodies as in the case of the Chilenia terrane (Ramos et al., 1986) or the Cuyania terrane (Ramos, 2004) at latitude 27°–38°S. A further proof for the presence of allochthonous terranes is the metamorphic evolution particularly of high pressure metamorphic rocks within the proposed suture zones of these microcontinents in the Andean basement (e.g. Casquet et al., 2001; Massonne and Calderón, 2008; Willner et al., 2011; Martínez et al., 2012; Massonne and Toulkeridis, 2012). A similar situation occurs in the Eastern Cordillera of Perú (Ramos, 2009), where the Ordovician magmatic arc is displaced from its position along the southern Peruvian coast towards a position considerably further inland (Fig. 1a). The Ordovician arc is represented within a metamorphic basement, part of the Marañon Complex (MC; Cardona et al., 2009; Chew et al., 2008). On the western border of this metamorphic complex, a chain of few small ultramafic bodies occurs which are scattered within the metamorphic basement (Fig. 1b). The biggest is represented by the Tapo Ultramafic Massif (TUM) near Tarma in the eastern Cordillera, which contains serpentinized peridotite, metagabbro with ocean ridge or ocean island chemical characteristics and podiform

* Corresponding author. Institut für Mineralogie und Kristallchemie, Universität Stuttgart, Azenbergstr. 18, 70174 Stuttgart, Germany. Tel.: +49 234 3224577; fax: +49 234 3214433.
E-mail address: arne.willner@rub.de (A.P. Willner).

http://dx.doi.org/10.1016/j.jsames.2014.05.001

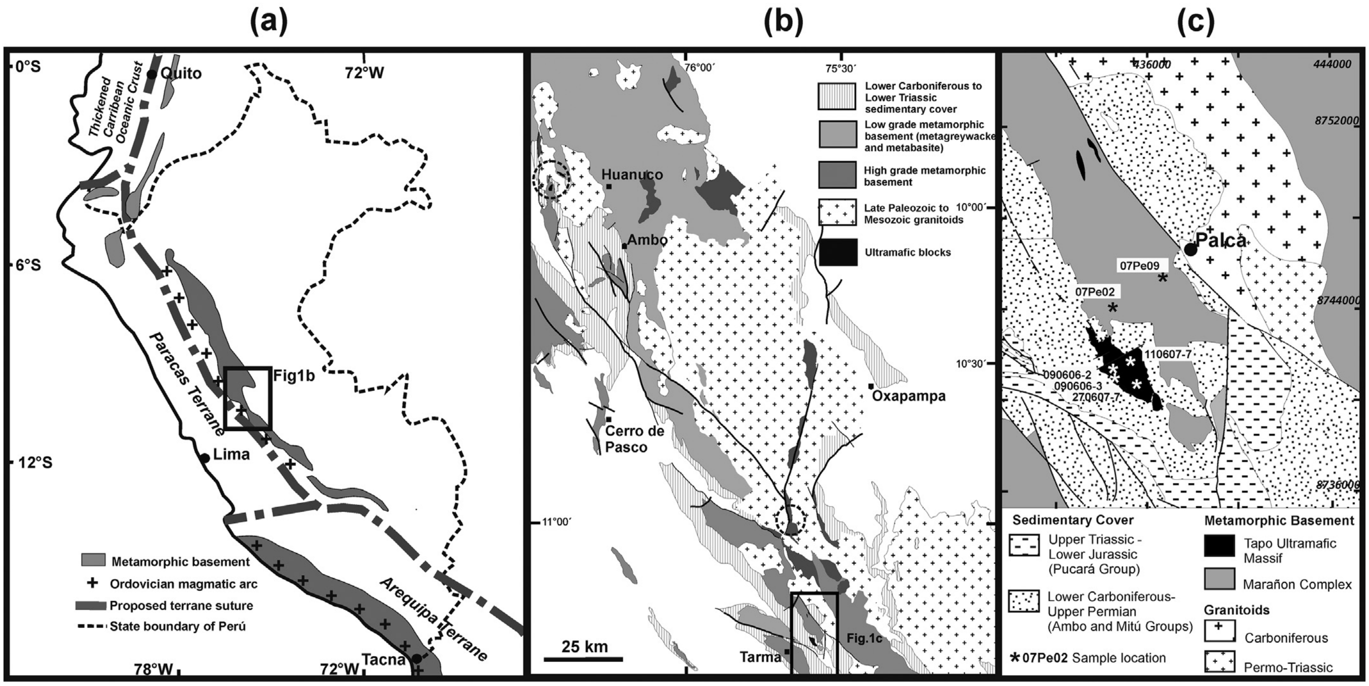

Fig. 1. (a) Geodynamic interpretation of the pre-Andean basement in Perú after Ramos (2009) and location of the target area. (b) Geological map of the basement of the Eastern Cordillera between Tarma and Huanaco (after Tassinari et al., 2011). (c) Geological map of the sample area east of Tarma (after Tassinari et al., 2011). Coordinates refer to the Peruvian National Grid.

chromitite lenses interpreted as an ophiolitic remnant (Castroviejo et al., 2009a, b; Tassinari et al., 2011). Due to the occurrence of this chain of ultramafic rocks, Ramos (2009) proposed an early Ordovician collision of an exotic Paracas terrane with Gondwana at a suture zone along the entire length of the Peruvian Eastern Cordillera. As a relic of this terrane a metamorphic basement block is observed in the continental shelf (Ramos and Aleman, 2000). By contrast, Chew et al. (2007) and Cardona et al. (2009) proposed a mere original embayment on the western Gondwanan margin during early Palaeozoic times. However, more recently Romero et al. (2013) confirmed the existence of a metamorphic crustal basement in the present Peruvian forearc by abundant U/Pb dating of zircon. These data indicate a likely Grenville-age high-grade metamorphism and an Ordovician magmatic event similar to the Arequipa Massif further south.

Here we will provide first quantitative PT-data from rocks of two adjacent contrasting metamorphic complexes (TUM and MC; Table 1) along the suture zone to test the collision scenario (Fig. 1c). Furthermore we try to date the peak of metamorphism in the TUM for the first time and correlate this age with existing ages in the MC. The aim is to provide further understanding about the mechanisms of collision zones of microplates in general.

2. Geological setting

An extensive, but discontinuous 500 km long chain of pre-Mesozoic metamorphic units forms the basement of the Peruvian Eastern Cordillera (Fig. 1a). This collage of heterogeneous metamorphic units was first described as Marañon Complex (MC) by Wilson and Reyes (1964) and Dalmayrac et al. (1980). It mainly contains various low- to medium-grade metamorphic units of volcanosedimentary origin and some high-grade domains of restricted extent. The complex is unconformably overlain by fossiliferous Carboniferous and Permian sedimentary rocks (Dalmayrac et al., 1980). Ordovician and Carboniferous sedimentation ages were proposed by Chew et al. (2007, 2008) and Cardona et al. (2009) due to detection of youngest magmatic zircon ages in the detrital zircon spectra of metasandstone from different parts of the MC with age ranges of 484–442Ma and 368–324 Ma, respectively. In the Tarma area low grade metasedimentary rocks and metavolcanic rocks of the MC were mapped by Megard et al. (1996) as Huacár Group. These authors proposed a Precambrian age of metamorphism for these metasediments of terrigenous origin. However, Chew et al. (2007) dated the Pacococha Adamellite intrusion north of Tarma into the western MC at 474 ± 3 Ma (U/Pb zircon). Similar ages of 442–445 Ma were obtained by Chew et al. (2007) for granitoid intrusions in the western MC in northern Perú, where also youngest zircon of Ordovician age occurs as detritus in the metasediments of the MC. Zircon of a leucosome in garnet-bearing paragneisses from the western MC in northern Perú yielded an age of 478 ± 3 Ma (Chew et al., 2007). In the same region Cardona et al. (2009) reported an age of 484 ± 12 Ma for metamorphic overgrowth in zircon crystals. Thus, it is likely that the rocks of the western MC were deposited and metamorphosed

Table 1
Assemblages of the studied samples.

110607-7	Garnet–epidote–chlorite–titanite–ilmenite–clinopyroxene	Tapo Ultramafic Massif
090606-3	Amphibole–garnet–epidote–chlorite–albite–quartz–titanite–ilmenite–clinopyroxene	Tapo Ultramafic Massif
090606-2	Amphibole–garnet–epidote–chlorite–albite–quartz–titanite–ilmenite	Tapo Ultramafic Massif
270607-7	Amphibole–garnet-epidote–chlorite–albite–quartz–titanite–ilmenite	Tapo Ultramafic Massif
07Pe02	Amphibole–epidote–chlorite–albite–quartz-titanite	Marañon Complex
07Pe09	Chlorite–white mica–albite–quartz–ilmenite	Marañon Complex

during Ordovician times (Chew et al., 2007; Cardona et al., 2009). During the Carboniferous the MC was intruded by large granitoid plutons (307 ± 0.7 and 325 ± 0.6 Ma; U/Pb zircon; Chew et al., 2007). However, in the eastern MC youngest detrital zircon in the metasediments reveals a Carboniferous maximum sedimentation age for the metasediments (345 ± 14 Ma; Chew et al., 2007). It was suggested by Chew et al. (2007) and Cardona et al. (2009) that the eastern MC likely has a Carboniferous age of sedimentation and metamorphism. A similar situation with an Ordovician metamorphic belt in the western MC and a Carboniferous metamorphic belt in the eastern MC is also proposed for northern Perú (Chew et al., 2007; Cardona et al., 2009). The Ordovician western MC is unconformably overlain by a clastic continental series of conglomerate, sandstone and tuff (Ambo Group; Lower Carboniferous) and the eastern MC by the Upper Permian Mitu Group, a continental molasse sequence, which also overlies the Ambo Group with an erosive surface (Cardona et al., 2009). Both cover sequences are overlain by micritic limestone of the Upper Triassic–Lower Jurassic Pucará Group. This shows that crustal thickening and exhumation of the metamorphic rocks was considerably earlier in the western MC than in the eastern MC and the magmatic arc evidently migrated from west to east during late Palaeozoic times.

In the Tarma area three ultramafic bodies occur associated with the MC (Fig. 1b): (1) two smaller bodies are intercalated into schists of the western MC parallel to its predominant transposition foliation about 7 km NE of Acobamba (Megard et al., 1996; Castroviejo et al., 2009a,b). (2) Near the village of Tapo E of Tarma a major occurrence of 5 × 2 km extent is referred here as Tapo Ultramafic Massif (TUM; Tassinari et al., 2011). The occurrence was originally mapped as being thrust onto the Ambo Group in the east and being unconformably overlain by the Ambo Group in the west (Megard et al., 1996). However, Castroviejo et al. (2009a,b) and Tassinari et al. (2011) interpret the entire boundaries of the TUM as a discrete upper crustal nappe contact with intense cataclasis which was emplaced onto the structurally underlying sediments of the Ambo Group during post-Carboniferous times (Fig. 1c). The TUM mainly represents a lense-shaped serpentinite body, which also contains small podiform chromitite deposits, metagabbro and lenses of garnet amphibolite, which show penetrative ductile non-coaxial deformation. Kinematic indicators in the mylonitic foliation of garnet amphibolites (S–C structures; σ-clasts) with stretching lineations in an NNW-SSE direction indicate a top to the NNW sense of movement. The predominant transposition foliation dips towards the east in the entire TUM. The chemical composition of the metabasite suggests a mid-ocean ridge or an ocean island protolith. Hence the whole sequence was interpreted as a disrupted ophiolitic complex (Castroviejo et al., 2009a, b; Tassinari et al., 2011). This dismembered ophiolitic slice has a protolith age of 718 ± 47 Ma (Sm–Nd mineral isochron age; Tassinari et al., 2011). A first K–Ar age on metamorphic amphibole of 448 ± 26 Ma was interpreted by Tassinari et al. (2011) as cooling age of an Ordovician metamorphic event.

3. Analytical methods

Mineral compositions were obtained using a CAMECA SX 100 electron microprobe with 5 wavelength-dispersive systems at Universität Stuttgart, Germany. Operating conditions were an acceleration voltage of 15 kV, a beam current of 10 nA, 20 s counting time per element each on the peak and the background and preferably a slightly defocused beam of 5 μm in order to avoid loss of alkalies in mica and amphibole. The following standards were used: natural wollastonite (Si, Ca), synthetic periclase (Mg), synthetic corundum (Al), synthetic rutile (Ti), natural haematite (Fe), natural albite (Na), natural orthoclase (K), natural rhodonite (Mn) and natural baryte (Ba). The PAP correction procedure provided by Cameca was used for matrix corrections. Representative analyses and structural formulae of minerals used for P–T calculations, together with the calculation procedure of the structural formulae, are presented in the electronic data base at the JSAMES website and in Table 2.

Whole rock analyses of major elements were done from fused glass discs obtained by melting rock powder and spectromelt in the proportion 1:9. We used a PHILIPS PW2400 X-ray fluorescence spectrometer at Universität Stuttgart (samples 07Pe02 and 07Pe09) and Laboratorio Nacional de Energia e Geologia Porto (samples 090606-3, 090606-2, 270607-7, 110607-7) to analyse the glass disks. CO_2 and H_2O were determined in Stuttgart by infrared-spectroscopy using the C/H/H_2O-analyzer Leco RC-412. The analytical data used for the calculation of the P–T pseudosections presented in this paper are given in Table 3.

The isotopic analysis was carried out at Geochronological Research Center of University of São Paulo, Brazil. The Sm–Nd analysis was prepared by standard methods according to the analytical procedures described by Sato et al. (1995). Each sample was ultrasonically washed in triple distilled water, before chemical attack, and all samples were totally digested with $HF_{(conc.)}$ plus $HNO_{3(conc.)}$ in a proportion 2:1 using Parr type bombs. Then the solutes were evaporated to dryness and converted to chloride form with 2.62 N HCl. Samples for Sm–Nd analyses were spiked with a ^{150}Nd–^{149}Sm spike. The solutes were evaporated, converted with 0.2 ml 2.5 N HCl and the rare earth elements (REE) were separated with 6.2 N HCl in a AG 50WX8, 200–400 mesh cationic exchange resin. Afterwards, the solutions were dried and eluted with 0.26 N HCl and Sm was collected with 0.55 N HCl. Both elements were loaded as phosphates on Re filaments and analysed in the 262 Finnigan-Mat mass spectrometer. Measurements of ^{143}Nd/^{144}Nd were normalized to ^{146}Nd/^{144}Nd = 0.719. The averages of ^{143}Nd/^{144}Nd for La Jolla and BCR-1 standards were 0.511847 ± 0.00005 (2σ) and 0.512662 ± 0.00005 (2σ) respectively. The blanks of Nd were less than 0.03 ng. The Sm–Nd isochronic age was calculated using the program ISOPLOT, Ludwig (2009). Data are presented in Table 4.

4. Petrography and mineral chemistry

4.1. Tapo Ultramafic Massif (TUM)

We selected three garnet amphibolite samples (090606-2, 090606-3 and 270607-7) from the TUM, which contain the assemblage garnet–Ca–amphibole–epidote–chlorite–albite–quartz–titanite–ilmenite (Table 1). This assemblage points to conditions of the albite–epidote–amphibolite facies. Magmatic clinopyroxene relics can be observed in weakly foliated garnet amphibolite 090606-3 and a metaultrabasite 270607-5.3, which is associated with the garnet amphibolite. Unoriented clinopyroxene as well as deformed and recrystallized plagioclase of 1–3 mm size point to a relict plutonic fabric of a former gabbro, whereas the metaultrabasite can be interpreted as a former cumulate. On the other hand garnet amphibolite samples 090606-2 and 270607-7 are strongly foliated (Fig. 2). Foliation is defined by 0.5–1 mm thick layers that are mono-, bi- or trimineralic. Amphibole, titanite and epidote may form monomineralic layers, whereas amphibole–chlorite, garnet–chlorite, epidote–quartz form typical bimineralic layers. Thin 0.2–0.6 mm thick titanite trails that contain grains of 0.1 mm size show a characteristic transposition fabric with tight and rootless intrafolial folds. Although most epidote, amphibole and chlorite (0.2–1 mm) are oriented parallel to the foliation, unoriented grains of these minerals are crosscutting. This points to static recrystallisation after formation of the foliation similar to a typical polygonal fabric in quartz-albite or

Table 2
Representative mineral compositions.

Garnet	090606-2			
	Core		Rim	
SiO_2	37.6	Calc.	37.7	35.0
Al_2O_3	21.3	12.4 kb	21.0	7.08
TiO_2	0.16	500 °C	0.16	3.12
Fe_2O_3	0.55		1.05	19.1
FeO	22.1		26.1	0.00
MnO	4.92		1.31	0.17
MgO	0.32		0.66	0.06
CaO	14.0		13.3	34.0
Sum	101.0		101.3	98.6
Si	5.943	6.000	5.945	5.776
Alt	0.057		0.055	0.224
SU0	6.000		6.000	6.000
Alo	3.915	4.000	3.856	1.152
Fe^{3+}	0.066		0.125	2.373
Ti	0.019		0.019	0.387
SU1	4.000		4.000	3.912
Fe^{2+}	2.918	2.760	3.445	0.000
Mn	0.659	0.780	0.175	0.023
Ca	2.367	2.340	2.243	6.014
Mg	0.076	0.120	0.155	0.014
SU2	6.019	6.000	6.018	6.051

Amphibole				
110607-7	090606-2		07Pe02	
SiO_2	48.2	Calc.	53.0	Calc.
Al_2O_3	6.99	12.4 kb	2.11	2.5 kb
TiO_2	0.10	500 °C	0.05	320 °C
Fe_2O_3	4.85		3.55	
FeO′	13.6		13.7	
MgO	10.6		13.0	
CaO	10.9		11.9	
K_2O	0.07		0.11	
Na_2O	1.36		0.34	
MnO	0.15		0.37	
H_2O'	2.02		2.06	
Sum	98.9		100.1	
Si	7.166	7.680	7.709	7.920
Alt	0.834	0.320	0.291	0.080
sum	8.000	8.000	8.000	8.000
Alo	0.389	0.320	0.070	0.040
Ti	0.012		0.005	
Mn	0.019		0.045	
Fe^{3+}	0.542		0.389	
Fe^{2+}	1.689	2.430	1.666	1.980
Mg	2.350	2.250	2.824	2.980
Sum	13.000	5.000	13.000	5.000
Ca	1.737	1.920	1.853	2.000
Na	0.392	0.080	0.095	
K	0.012		0.020	
Sum	2.142	2.000	1.968	2.000
OH	2.000	2.000	2	2.000

White mica		
	07Pe09	
SiO_2	48.4	
Al_2O_3	28.8	
TiO_2	0.41	
Fe_2O_3	1.10	
FeO′	3.80	
MgO	2.16	
MnO	0.04	
CaO	0.02	
BaO	0.13	
Na_2O	0.16	
K_2O	10.5	
H_2O'	4.45	
Sum	99.9	6.540
Si	6.515	1.460
Alt	1.485	8.000
Sut	8.000	3.400
Alo	3.079	
Ti	0.042	
Fe^{3+}	0.112	0.240
Fe^{2+}	0.429	
Mn	0.005	0.300
Mg	0.434	
Suo	4.100	
Ba	0.007	
Ca	0.003	0.040
Na	0.042	1.960
K	1.801	2.000
Suz	1.853	4.000
OH	4.000	

Chlorite	090606-2		07Pe02		07Pe09	
SiO_2	24.99	Calc.	25.61	Calc.	23.99	Calc.
Al_2O_3	19.6	12.4 kb	20.6	2.5 kb	20.8	2.5 kb
TiO_2	0.01	500 °C	0.06	320 °C	0.03	320 °C
FeO	28.6		27.9		19.2	
MgO	12.9		14.7		20.7	
MnO	0.38		0.42		0.87	
CaO	0.08		0.06		0.01	
H_2O'	11.0		11.4		11.3	
Sum	97.5		100.8		97.0	
Si	5.459	5.960	5.373	6.000	5.070	6.000
Alt	2.541	2.040	2.627	2.000	2.930	2.000
Alo	2.503	2.040	2.477	2.000	2.260	2.000
Ti	0.001		0.010		0.004	
Mn	0.070	0.040	0.074	0.100	0.155	
Fe	5.228	5.780	4.893	5.760	3.394	5.700
Mg	4.197	4.140	4.588	4.140	6.511	4.300
Suo	11.999	12.000	12.042	12.000	12.325	12.000
Ca	0.018		0.014		0.002	
OH	16.000	16.000	16.000	16.000	16.000	16.000

Epidote				
	090606-2		07Pe02	
SiO_2	37.5	Calc.	38.5	Calc.
Al_2O_3	23.5	12.4 kb	27.0	2.5 kb
Fe_2O_3	13.6	500 °C	9.70	320 °C
Mn2O3	0.13		0.21	
TiO_2	0.03		0.08	
CaO	23.1		23.2	
H2O'	1.87		1.92	
Sum	99.7		100.5	
Si	3.000	3.000	3.000	3.000
Al	2.218	2.360	2.480	2.720
Ti	0.002		0.005	
Mn	0.008		0.013	
Fe	0.817	0.640	0.570	0.280
sum	3.044	3.000	3.067	3.000
Ca	1.980	2.000	1.936	2.000
OH	1.000	1.000	1.000	1.000

Clinopyroxene		
	90606-2	110607-7
SiO_2	51.4	53.1
Al_2O_3	0.51	0.04
TiO_2	0.02	0.00
Fe_2O_3	2.63	2.29
FeO'	10.2	4.07
MnO	0.21	0.12
MgO	10.7	15.3
CaO	24.0	25.0
Na2O	0.24	0.00
Sum	100.0	100.0
Si	1.959	1.967
Alt	0.023	0.002
SU1	1.982	1.969
Alo	0.000	0.000
Ti	0.001	0.000
Fe3+	0.075	0.064

Titanite		
	090606-2	07Pe02
SiO_2	29.7	30.7
TiO_2	38.5	38.1
Al_2O_3	0.796	1.62
Fe_2O_3	1.29	1.328
MnO	0.044	0.045
MgO	0	0.022
CaO	27.4	28.3
H2O'	0.143	0.149
Sum	98.89	100.3
Si	0.992	1.005
Ti	0.965	0.936
Al	0.031	0.051
Fe	0.032	0.014
Mn	0.001	0.001
Mg	0	0.001
Ca	0.978	0.991

O'	12.047	12.000	12.039	12.000	Fe2+	0.326	0.126	O'	4.987	4.966
					Mn	0.007	0.004	OH	0.032	0.032
					Mg	0.610	0.845	Sum	5.018	4.999
					Ca	0.982	0.993			
					Na	0.018	0.000			
					SU2	2.018	2.031			

Garnet: cations based on 48 negative charges including 10 cations in the tetrahedral and octahedral site to calculate Fe^{3+}.
Amphibole: proportion of cations is based on the sum of cations = 13 except for Ca, Na and K for estimation of Fe^{3+} and on 46 negative charges.
White mica: the proportion of cations is based on 42 negative charges neglecting the interlayer cations; the sum of octahedrally coordinated cations is set at 4.1 to allow for an estimation of Fe^{3+}.
Chlorite: cations based on 56 negative charges; H_2O calculated on the basis of OH = 16.
Epidote: proportions of cations are based on normalization of Si to three cations.
Clinopyroxene: normalization based on 6 negative charges.
Titanite: sum of cations = 3; OH = (Al + Fe) × 0.5; O' = [(Σ positive charges) − OH] × 0.5.

quartz-epidote (0.1–0.5 mm) layers. Occasional shear bands and brittle fissures are restricted features of late deformation. Garnet grains of 0.3–0.7 mm size are generally idioblastic, but can be replaced by chlorite at the rims (Fig. 2d).

The garnet is essentially an almandine-grossular solid solution (almandine$_{0.46-0.62}$grossular$_{0.25-0.45}$pyrope$_{0.01-0.18}$spessartite$_{0.02-0.11}$). Almandine and pyrope contents increase from core to rim, whereas spessartite decreases and grossular contents show little variation. Amphibole compositions vary strongly between samples (Table 2; Fig. 3a): in sample 090606-3 amphibole is actinolite to magnesiohornblende (Na 0.10–0.66 apfu, Na_A 0.00–0.66 apfu, X_{Mg} 0.42–0.68), in sample 270607-7 magnesiohornblende to tschermakite (Na 0.58–1.03 apfu, Na_A 0.36–0.82 apfu, X_{Mg} 0.25–0.46) and in sample 090606-2 tschermakitic hornblende to tschermakite (Na 0.05–0.80 apfu, Na_A 0.3–0.5 apfu, X_{Mg} 0.41–0.58). There is a slight trend of decreasing Si contents from core to rim. Epidote composition within all samples varies strongly ($X_{pistacite}$ = 0.4–0.9) contrasting that of chlorite (Si 5.3–5.7 apfu; X_{Mg} 0.35–0.51). Clinopyroxene composition is diopside$_{0.56-0.58}$hedenbergite$_{0.20-0.30}$acmite$_{0.07-0.10}$orthopyroxene$_{0.02-0.05}$ tschermak-component$_{0.02-0.07}$. Plagioclase is invariably albite.

For radiometric age dating we selected a rodingite (sample 110607-007) intercalated as small lenses in serpentinite. Its whole rock composition is remarkable due to its low SiO_2 content (29 wt%; Table 1), but high contents of CaO (15.5 wt%), FeO (22 wt%) and TiO_2 (6.8 wt%). This rock contains about 60–65% garnet in clusters of polygonal coarse grains apart from chlorite and clinopyroxene in the predominant assemblage and ilmenite, titanite and apatite as accessories. Crosscutting fissures contain garnet, chlorite and clinopyroxene. The rock shows a strong tendency of phase reduction particularly regarding the predominant garnet. This points to a typical metasomatic rock type.

Garnet is a complex grandite solid solution (andradite$_{0.41-0.71}$grossular$_{0.18-0.36}$morimotoite$_{0.01-0.20}$pyrope$_{0.00-0.04}$Al-schorlomite$_{0.00-0.04}$katoite$_{0.02-0.03}$almandine$_{0.00-0.03}$Mg-morimotoite$_{0.00-0.02}$spessartite$_{0.00-0.01}$; calculation according to Locock, 2008). There is no marked core-rim compositional zonation, but compositions tend to oscillate. Clinopyroxene is diopside with 17–37% hedenbergite component. Chlorite is relatively homogeneous (Si 5.53–5.89 apfu) with some Mn-content (0.02–0.04 apfu).

4.2. Marañon complex (MC)

For comparison we selected two different rock types from the western MC, which is supposed to represent an Ordovician magmatic arc: the phyllite sample 07Pe09 and the greenschist sample 07Pe02 are low grade rocks below the garnet isograde collected along a road cut west of Palca (Fig. 1c). Medium-grade metamorphic rocks exceeding the garnet isograde occur east of Palca. We did not consider those rocks, because they likely belong to a younger Carboniferous metamorphic event.

The greenschist facies rocks of the western MC are characterized by the absence of garnet and the presence of albite: the phyllite 07Pe09 contains the assemblage white mica–chlorite–albite–quartz–ilmenite, the metabasite 07Pe02 the assemblage Ca-amphibole–epidote–chlorite–albite–quartz–titanite. Chlorite, white mica and amphibole are oriented parallel to the predominant foliation which is characterized by an internal crenulation in the metapelite. In the metabasite, the foliation is a compositional banding with alternating bands of (1) titanite, (2) epidote–chlorite and (3) amphibole–chlorite–quartz. Quartz and epidote recrystallized as fine-grained polygonal aggregates. Some

Table 3
Whole rock analyses.

	(a) Original analyses					(b) Recalculated for pseudosections		
	Samples Tapo ultramafic Massif							
	090606-3	090606-2	270607-7	110607-7		090606-3	090606-2	270607-7
SiO_2	49.4	40.0	40.4	29.4	SiO_2	47.3	41.5	39.3
TiO_2	2.57	3.26	5.09	6.79	TiO_2	2.46	3.38	4.95
Al_2O_3	11.6	10.1	11.0	10.2	Al_2O_3	11.0	10.5	10.7
Fe_2O_3	14.1	21.9	23.4	22.3	FeO	12.2	20.4	20.5
MnO	0.15	0.18	0.25	0.64	MnO	0.14	0.19	0.24
CaO	10.8	8.11	8.88	17.5	CaO	10.4	8.41	8.65
MgO	6.80	7.96	6.82	8.32	MgO	6.50	8.26	6.65
Na_2O	3.06	0.22	1.97		Na_2O	2.93	0.23	1.92
K_2O	0.12	0.06	0.12		H_2O	7.00	7.00	7.00
P_2O_3	0.13	0.01	<0.050	0.01	O_2	0.10	0.10	0.10
LOI	1.03	8.03	2.18	4.83		100.0	100.0	100.0
Sum	99.8	99.8	100.0	100.0				
	07PE02		07PE09				07PE02	07PE09
Samples western Marañon complex								
SiO_2	48.6		62.7		SiO_2		47.1	60.6
TiO_2	1.84		0.65		TiO_2		1.79	0.63
Al_2O_3	14.2		16.5		Al_2O_3		13.7	15.9
Fe_2O_3	13.9		6.90		FeO		12.1	6.0
MnO	0.22		0.13		MnO		0.21	0.12
MgO	6.13		2.56		MgO		5.94	2.47
CaO	10.4		0.86		CaO		10.0	0.8
Na_2O	1.94		1.47		Na_2O		1.88	1.42
K_2O	0.06		4.56		K_2O		0.00	4.41
P_2O_3	0.17		0.11		CO_2			0.59
CO_2			0.61		H_2O		7.00	7.00
H_2O	3.33		2.98		O_2		0.10	
	100.7		100.0				100.0	100.0

Table 4
Sm–Nd analytical results.

Sample	Material	Sm (ppm)	Nd (ppm)	$^{147}Sm/^{144}Nd$	Error	$^{143}Nd/^{144}Nd$	Error (2σ)
11-0607-7	WHOLE-ROCK	3.948	9.858	0.2422	0.0015	0.513221	0.000015
11-0607-7	CHLORITE	3.387	6.637	0.3086	0.0019	0.513438	0.000014
11-0607-7	GARNET	8.432	13.046	0.3908	0.0027	0.513673	0.000016

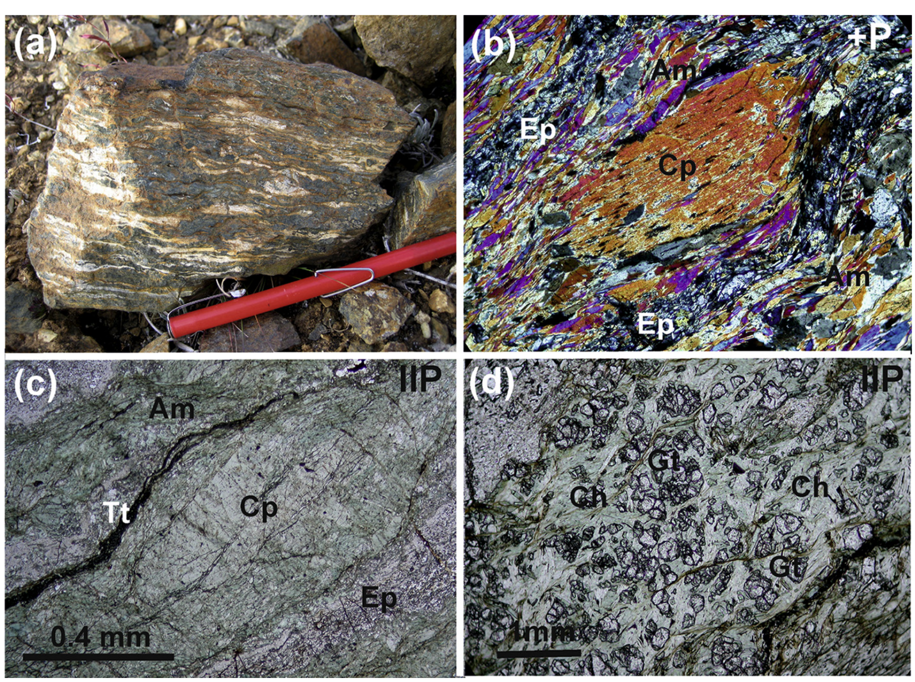

Fig. 2. Garnet amphibolite of the TUM: (a) strongly foliated hand specimen (sample 270607-7); (b–d) microphotographs of sample 090609-2; +P crossed polars; IIP parallel polars; abbreviations as in Fig. 4.

coarse amphibole crystals in the metabasite are partly rotated indicating a slight non-coaxial overprint.

Amphibole in the metabasite is actinolite (Na 0.10–0.22 apfu, X_{Mg} 0.51–0.60; Fig. 3a), epidote contains 57–92 mol % pistacite component and chlorite has a rather restricted compositional variation (Si 5.28–5.38 apfu, X_{Mg} 0.48–0.49). White mica in the metapelite is muscovite with Si contents of 3.14–3.26 apfu and a composition that strongly deviates from the ideal Tschermak substitution line due to enhanced Fe^{3+} substitution (calculated Fe^{3+} 0.06–0.23 apfu; Table 2; Fig. 3b).

5. Geothermobarometry

5.1. The calculation method

Based on the bulk rock composition, we calculated PT pseudosections for three garnet amphibolite samples from the TUM (samples 090606-2, 090606-3 and 270607-7; Fig. 1c) and additionally for a metabasite sample (samples 07Pe02) and a metapelite (sample 07Pe09) from the MC for comparison (Fig. 1c). Samples were chosen from those rocks without signs of metasomatism or veining, where the dominating peak metamorphic assemblage is homogenously distributed at thin section and outcrop scale. We used the PERPLE_X software package (Connolly, 1990, 2005; used version of august 2006) and the thermodynamic data set of Holland and Powell (1998) (updated 2002) for minerals and aqueous fluid.

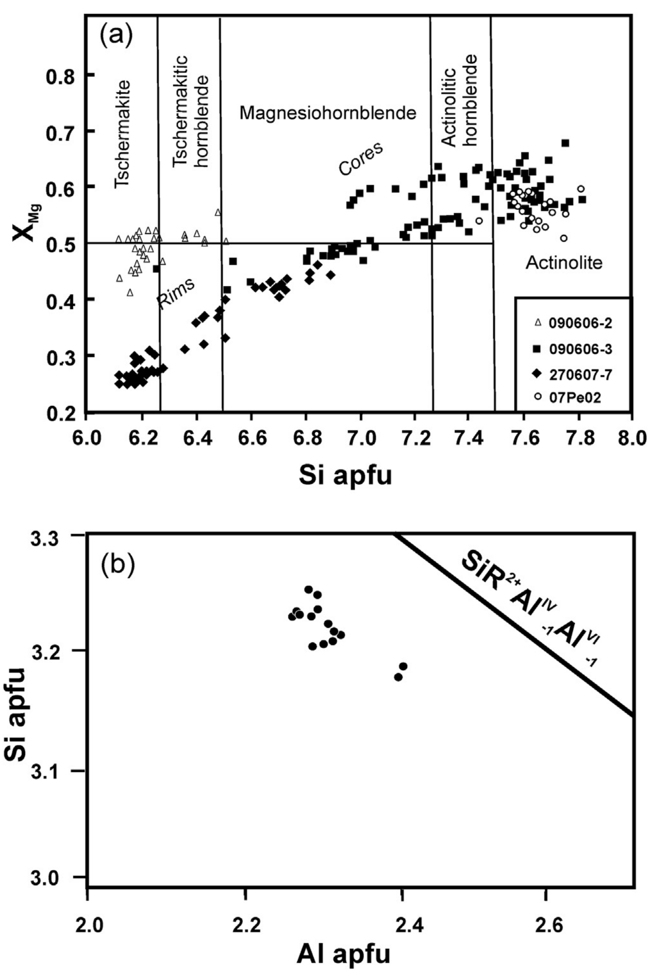

Fig. 3. (a) X_{Mg}–Si variation of amphibole in garnet amphibolite; (b) Si–Al variation of white mica in phyllite (sample 07Pe09).

Calculations were performed using the following solid-solution models: for white-mica, epidote, garnet, plagioclase, amphibole, omphacite, chlorite and biotite by Holland and Powell (2003) and Powell and Holland (1999). Albite, K-feldspar, quartz, titanite, H_2O and paragonite were considered as pure phases. For the calculation of the pseudosections the major element compositions analysed by XRF were simplified to a 10-component system (SiO_2–TiO_2–Al_2O_3–FeO–MgO–MnO–CaO–Na_2O–H_2O–O_2) for the garnet amphibolite samples and to an 11-component system (SiO_2–TiO_2–Al_2O_3–FeO–MgO–MnO–CaO–Na_2O–K_2O–H_2O–O_2) for the metabasite and (SiO_2–TiO_2–Al_2O_3–FeO–MgO–MnO–CaO–Na_2O–K_2O–H_2O–CO_2) for the metapelite, all normalized to 100% (Table 3). Water contents were augmented to excess water conditions considered to have prevailed during peak PT conditions. Oxygen contents were estimated (0.04, respectively, 0.1 wt %) to account for epidote and magnetite present in the samples. Calculated compositions of minerals provide good coincidence with measured ones (Table 2) except for amphibole, because solid solution models for amphibole are still not optimal.

5.2. Tapo Ultramafic Massif

PT pseudosections were calculated for three selected garnet amphibolite samples with similar results (Figs. 4 and 5). A PT field for the position of the observed assemblage (chlorite–amphibole–garnet–epidote–titanite–ilmenite–quartz) in sample 090606-2 is calculated outside the stability field of albite above 7 kbar, 450 °C (Fig. 4). Hence the observed albite must be regarded as a late phase formed during decompression. To higher pressures the PT field of the observed assemblage is limited by the appearance of omphacite between 9 and 15 kbar, to higher temperature by the appearance of rutile above 520 °C. The fields of the observed assemblages in samples 090606-3 and 270607-7 are more restricted to about 9–13 kbar, 450–500 °C (Fig. 5). However, in these rocks garnet would be predicted also to appear within the stability field of albite. The PT ranges for the appearance of omphacite and rutile are similar to sample 090606-2. The maximum pressure conditions reached can be much further restricted by the intersection of the calculated isopleths for the four major components of the garnet core compositions (almandine, pyrope, grossular, spessartite). Due to uncertainties about the exact core composition usually a restricted PT field occurs. This is plotted for the three amphibolite samples in Fig. 5. The calculated PT fields are remarkably similar and the most optimal overlap points to a maximum PT range of 11–13 kbar/500–540 °C. This suggests similar PT conditions for the rocks of the TUM. The internal element zonation in garnet suggests slight decompression and heating during garnet growth. Hence above derived conditions for the garnet core represent peak pressure conditions, whereas the garnet rims represent peak temperature conditions around 600 °C.

5.3. Western Marañon complex

For metapelite sample 07Pe09 a PT pseudosection was calculated and the maximum PT conditions can be restricted to low pressures and temperatures as follows (Fig. 6a): The observed assemblage chlorite–white mica–quartz–albite–carbonate is limited to temperatures below 330 °C, when biotite would appear. Above 420–450 °C plagioclase of oligoclase composition would be present. The calculated Si isopleth of the maximum Si-content observed for white mica (3.26 apfu) restricts the maximum PT conditions to 2.4–2.6 kbar, 300–330 °C. The calculated appearance of K-feldspar in the pseudosection at these conditions could not be proved by observation in the thin section. The calculated PT pseudosection for greenschist sample 07Pe02 shows that the observed

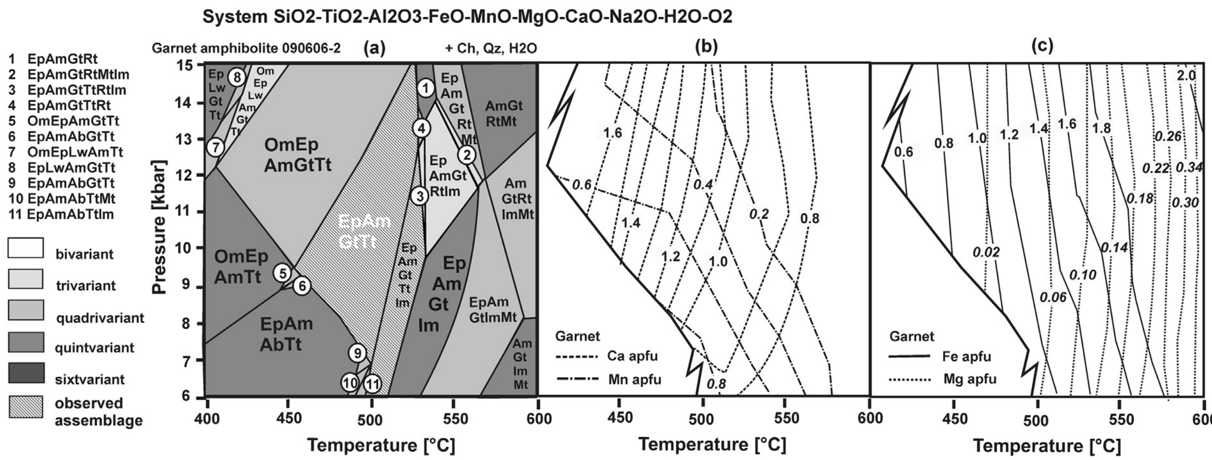

Fig. 4. (a) PT pseudosection of garnet amphibolite sample 090609-2 from the Tapo Ultramafic Complex; abbreviations: Am – amphibole; Ch – chlorite; Cp – clinopyroxene; Ep – epidote; Gt – garnet; Im – Ilmenite; Lw – lawsonite; Om – omphacite; Mt – magnetite; Qz – quartz; Rt – rutile; Tt – titanite (b) Ca, Mn – isopleths for garnet; (c) Fe, Mg – isopleths for garnet.

assemblage would be realized at the derived peak metamorphic conditions for the western MC. The calculated amphibole composition is in good agreement with the observed one (Table 2).

6. Geochronology

The analytical data of Sm–Nd isotopic analyses are shown in Table 4. Three analyses of the chlorite, garnet and whole rock for the rodingite sample 110607-07 were performed. These analyses yield $^{147}Sm/^{144}Nd$ ratios of 0.3086, 0.3908 and 0.2422 respectively and $^{143}Nd/^{144}Nd$ of 0.513438, 0.513673 and 0.513221, respectively. These isotopic ratios define a line on Sm–Nd isochronic diagram, with a slope that corresponds to an age of 465 ± 24 Ma with an initial $^{143}Nd/^{144}Nd$ of 0.512488 ± 0.000049 and MSWD value of 2.5 (Fig. 7). The defined Sm–Nd isochron age can be interpreted as the age of the metamorphic episode at near the temperature of 600 °C. The isochron proves an isotopic equilibrium in a strongly metasomatized rock. The age represents an age of a very time-restricted pulse of fluid influx into the disrupted ultramafic body along major shear zones. The fluid influx must be related to the peak of metamorphism within and outside of the ultramafic body, because medium-grade metamorphism released substantial amounts of hydrous fluids in equilibrium with pelitic and basic rock types that led to substantial metasomatism in the ultrabasic rocks with strongly contrasting whole rock compositions.

7. Discussion

Applying pseudosection techniques to garnet amphibolite in the TUM we can restrict its peak metamorphic pressure conditions to 12.0 ± 1 kbar and 520 ± 20 °C corresponding to 39–46 km burial depth (calculating with a mean crustal density of 2.8 g/ccm) and a low metamorphic geotherm of 12–13 °C/km. The peak of this metamorphic event coincides with the age of major influx of hydrous fluids in the TUM ultramafic rocks at 465 ± 24 Ma dated by the Sm–Nd mineral isochrone for the TUM rodingite. The K/Ar age of 448 ± 26 obtained for amphibole from TUM rocks by Tassinari et al. (2011) largely overlaps with the Sm–Nd age. A cooling age below the closure temperature of the K/Ar system for hornblende at ca. 500 °C appears unlikely, because peak temperatures hardly exceeded those of the closure temperature. We propose that ages rather represent ages of peak of metamorphism and related release of hydrous fluids by dehydration. This is certainly not a time-restricted event, but rather an age interval during Middle to Upper Ordovician times (ca. 470–440 Ma)

The detected high-pressure metamorphism indicates that the ophiolitic relic body, as the TUM was interpreted by Castroviejo et al. (2009a,b) and Tassinari et al. (2011), was subducted at a convergent margin or submerged in a collision zone. Its present exposure as a possible upper crustal nappe structurally overlying Late Carboniferous continental sediments (Castroviejo et al., 2009a,b; Tassinari et al., 2011) is a mere effect of post-Carboniferous brittle deformation in the upper crust, but definitely not a proof of an emplacement by obduction.

Two possible tectonic environments can be envisaged for the occurrence of subducted ophiolitic slices with a high-pressure overprint (pressures exceeding 10 kbar). At continental margins material from the subduction channel can return by forced flow towards the surface being incorporated as exotic blocks within accretionary prisms which never exceed a thickness of about 40 km (ca. 10 kbar; Willner et al., 2004, 2005; Wakabayashi, 1990). On the other hand, ophiolitic material with a high-pressure overprint can occur within an exhumation channel between colliding continental blocks (Brown et al., 2006; Van Staal et al., 2007; Willner et al., 2011; Massonne and Toulkeridis, 2012; Baldwin et al., 2012), where it is exhumed from the root of the collision zone by forced flow. Strong ductile non-coaxial deformation as described for the rocks of the TUM above (see also Tassinari et al., 2011) are representative for both scenarios. Unfortunately the present allochthonous structural position of the TUM makes correlation with the western MC difficult. However, a far displacement of the possible upper crustal nappe is unlikely and correlation with the small ultramafic bodies that are intercalated within the western MC parallel to its predominant transposition foliation are conceivable.

Within an adjacent block of the western Marañon Complex between Tarma and Palca (Fig. 1c) conditions of 2.5 ± 0.5 kbar, 320 ± 20 °C were detected in a similar way for phyllite and greenschist. This reflects burial to 8–10 km depth only and a relatively high metamorphic geotherm of 32–40 °C/km, which can be expected within a magmatic arc. So far known ages of metamorphism and intrusions of granitoid plutons in the age range 484–442 Ma (see above; Cardona et al., 2009; Chew et al., 2007) coincide with the age range of high-pressure metamorphism detected in the TUM. Best interpretation of this relationship is the development of a collision zone in close vicinity to a magmatic belt

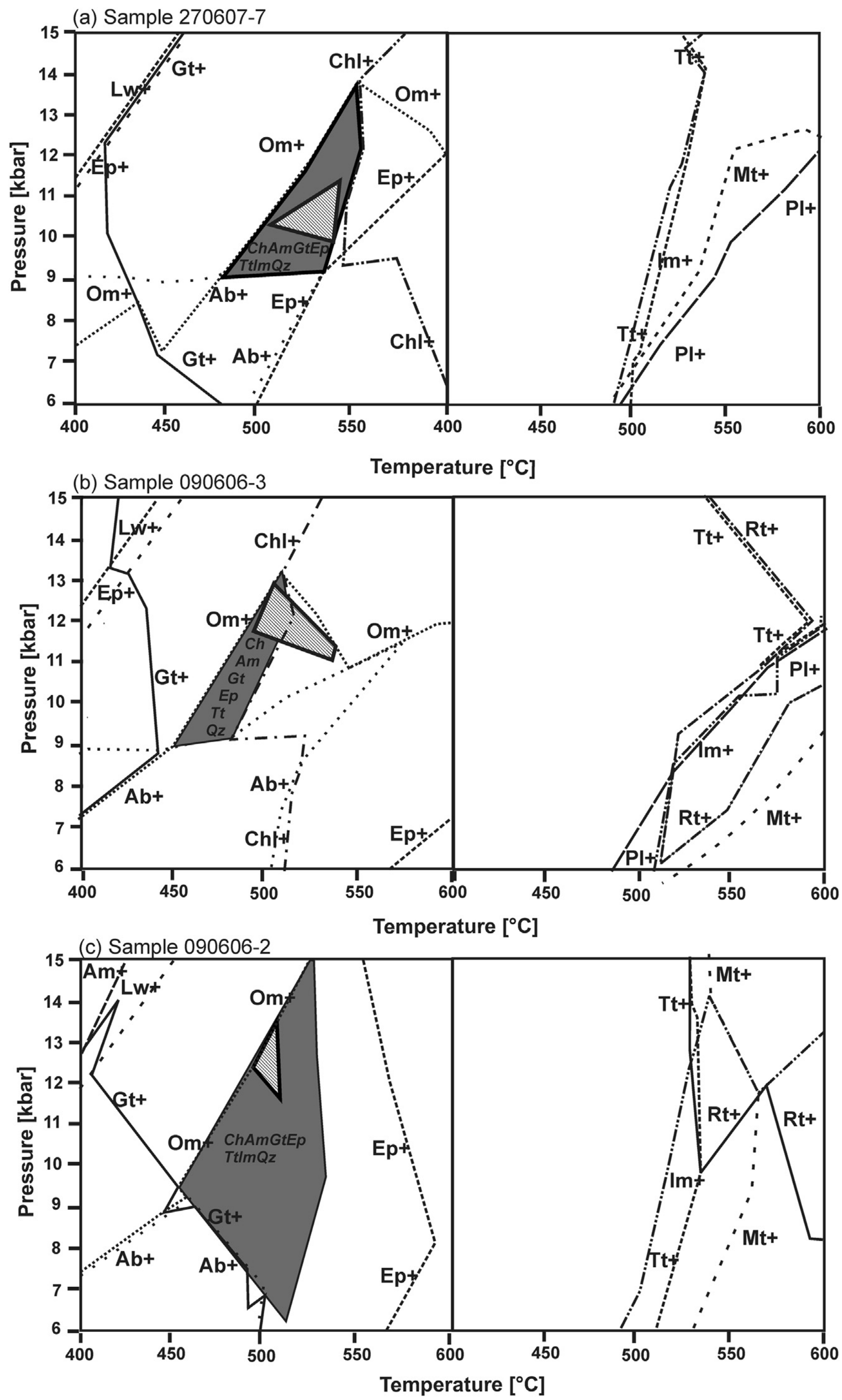

Fig. 5. PT fields of minerals extracted from calculated PT pseudosections based on the whole-rock compositions of three garnet amphibolite samples (270607-7; 090609-2; 090609.3; Table 3) from the Tapo Ultramafic Complex. Grey are the PT fields of the observed assemblages, hatched are the PT fields of the optimal intersection of compositional isopleths of garnet cores.

of a former active continental margin similar to the Ordovician collision zone of the Cuyania microplate in western Argentina, which developed late during the evolution of the Ordovician Famatinian magmatic arc in NW Argentina (Ramos, 2004, 2009). Moreover, an alternative to the collision of the Paracas microplate, as proposed by Ramos (2009) and Romero et al. (2013) would be a lateral growth of the continental margin in central and northern Perú by a frontal accretionary prism during post-Ordovician times. However, there is no indication of such scenario. Particularly high-pressure metamorphic rocks with pressures exceeding 10 kbar frequently evolve in continent-arc collision zones, as in the SW Urals (Brown et al., 2006), the Taconic collision within the peri-Laurentian margin in Newfoundland (Van Staal et al., 2007) or in New Guinea (Baldwin et al., 2012). Most of the continent-arc collisions are socalled "hard-collisions" (Zagorevski and van Staal, 2011): prior and during collision considerable thickening is generally developed in the overriding plate, which contains the arc, where most deformation occurs.

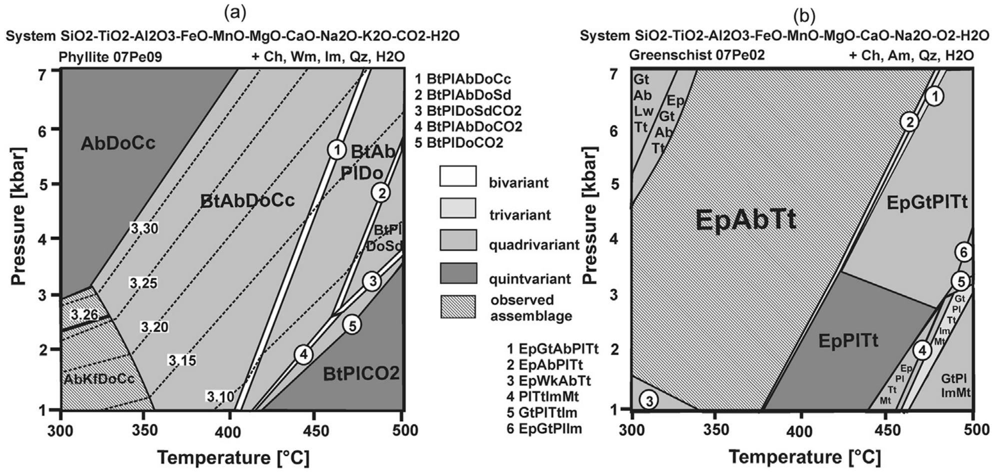

Fig. 6. PT pseudosections of (a) carbonate-bearing phyllite (07Pe09) and (b) greenschist (07Pe02) from the western Marañon Complex.

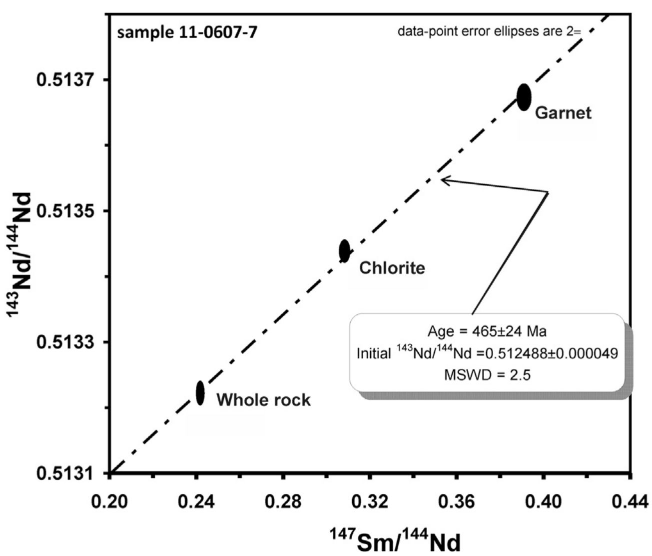

Fig. 7. Sm–Nd mineral isochron for rodingite sample 110607-7.

The top-to-NNW directed tectonic transport, which can be detected within the garnet amphibolite lenses would be consistent with an eastward dipping collision zone preceded by an eastward subduction causing the magmatic arc within the MC (Fig. 8). The exact position of the suture as well as the distribution of high and low-pressure domains in the MC still remain uncertain.

8. Conclusions

For the first time we recorded Ordovician high-pressure rocks in the Eastern Cordillera of Peru in close vicinity to coeval low-pressure rocks. The presence of high-pressure rocks exceeding 10 kbar associated with ultramafic complexes within an exhumation channel of a collision zone can be taken as a proof for the existence of an exotic Paracas terrane, which collided with a coeval magmatic arc at the former Peruvian margin of Gondwana during Ordovician times. U/Pb dating of zircon by Romero et al. (2013) revealed similar characteristics in rocks of the Paracas terrane in the present Peruvian forearc as in the Arequipa terrane further south (Fig. 1a). An important characteristic, for instance, is the evidence of an Grenvillian high temperature overprint. On the other

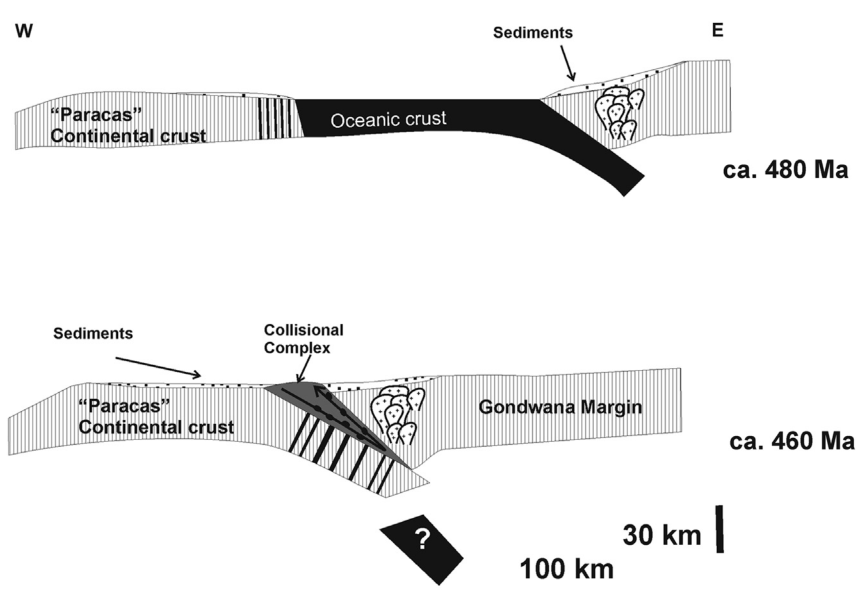

Fig. 8. Geodynamic scenario for the collision zone of the Paracas Terrane and the Marañon arc at the Ordovician continental margin of Western Gondwana in Perú.

hand, Grenvillian ages are not restricted to both terranes, but are prominent in detrital zircon age spectra in basement rocks throughout the Eastern Cordillera of Columbia, Ecuador and Perú (Chew et al., 2007, 2008; Mišković et al., 2009; Mišković and Schaltegger, 2009). The Paracas terrane was likely detached from the Amazonian margin during the break-up of Rodinia around 690 Ma and recollided during Ordovician times, whereas the Arequipa terrane stayed attached to Gondwana since its collision with Amazonia during the Grenville-Sunsas orogeny (Loewy et al., 2004).

Similar collisional settings can also be observed in the Eastern Cordillera of Ecuador (Massonne and Toulkeridis, 2012) and in Western Argentina (Casquet et al., 2001; Willner et al., 2011; Martínez et al., 2012). This shows that the collision of microcontinents which originated between the once coherent Laurentia and Gondwana during break-up of Rodinia, was an important feature during lateral continental growth of South America at the Pacific margin during Palaeozoic times.

Acknowledgements

Funding for field work (2006–2008) by Universidad Politecnica de Madrid (UPM) to RC (projects AL06-PID_010, AL07-PID_027, AL08-PID_025) is gratefully acknowledged. Furthermore we thank two anonymous reviewers for improvements, H.-J. Massonne for using the microprobe and XRF facilities at Institut für Mineralchemie und Kristallchemie of Universität Stuttgart (Germany), Th. Theye for assistance at the microprobe and Laboratorio Nacional de Energia e Geologia Porto (Portugal) for chemical analyses of rock samples.

Appendix A. Supplementary data

Supplementary data related to this article can be found at http://dx.doi.org/10.1016/j.jsames.2014.05.001.

References

Baldwin, S.L., Fitzgerald, P.G., Webb, L.E., 2012. Tectonics of the new Guinea region. Annu. Rev. Earth Planet. Sci. 40, 495–520.
Brown, D., Spadea, P., Puchkov, V., Alvarez-Maron, J., Herrington, R., Willner, A.P., Hetzel, R., Gorozhanina, Y., Juhlin, C., 2006. Arc continent collision in the Southern Urals. Earth Sci. Rev. 79, 261–287.
Cardona, A., Cordani, U.G., Ruiz, J., Valencia, V.A., Armstrong, R., Chew, D., Nutman, A., Sanchez, A.W., 2009. U–Pb zircon geochronology and Nd isotopic signatures of the pre-Mesozoic metamorphic basement of the Eastern Peruvian Andes: growth and provenance of a Late Neoproterozoic to Carboniferous accretionary orogen on the northwest margin of Gondwana. J. Geol. 117, 285–305.
Casquet, C., Baldo, E., Pankhurst, R.J., Rapela, C.W., Galindo, C., Fanning, C.M., Saavedra, J., 2001. Involvement of the Argentine Precordillera terrane in the Famatinian mobil belt: U/Pb SHRIMP and metamorphic evidence from the Sierra de Pie de Palo. Geology 29, 703–706.
Castroviejo, R., Rodrigues, J.F., Acosta, J., Pereira, E., Romero, D., Quispe, J., Espi, J.A., 2009a. Geología de las ultramafitas pre-andinas de Tapo y Acobamba, Tarma, Cordillera Oriental del Perú. Geogaceta 46, 7–10.
Castroviejo, R., Pereira, E., Rodrigues, J.F., Acosta, J., 2009b. Pre-Andean serpentinite-chromite orebodies in the Eastern Cordillera of Central Perú, Tarma province. In: Williams, et al. (Eds.), vol. 2, pp. 927–929.
Chew, D.M., Schaltegger, U., Košler, J., Whitehouse, M.J., Gutjahr, M., Spikings, R.A., Mišković, A., 2007. U-Pb geochronologic evidence for the evolution of the Gondwanan margin of the north-central Andes. Geol. Soc. Am. Bull. 119, 697–711.
Chew, D.M., Magna, T., Kirkland, C.L., Mišković, A., Cardona, A., Spikings, R., Schaltegger, U., 2008. Detrital zircon fingerprint of the Proto-Andes: evidence for a Neoproterozoic active margin? Precambrian Res. 167, 186–200.
Connolly, J.A.D., 1990. Multivariable phase diagrams; an algorithm based on generalized thermodynamics. Am. J. Sci. 290, 666–718.
Connolly, J.A.D., 2005. Computation of phase equilibria by linear programming: a tool for geodynamic modeling and its application to subduction zone decarbonation. Earth Planet. Sci. Lett. 236, 524–541.
Dalmayrac, B., Laubacher, G., Marocco, R., 1980. Géologie des Andes Péruviennes. Caractères Généraux de l'Évolution Géologique des Andes Péruviennes: Paris. In: Travaux et Document de L'Office de la Recherché Scientifique et Tech.nique Outremer, vol. 122, p. 501.
Holland, T.J.B., Powell, R., 1998. An internally consistent thermodynamic data set for phases of petrological interest. J. Metamorph. Geol. 16, 309–343.
Holland, T.J.B., Powell, R., 2003. Activity–composition relations for phases in petrological calculations: an asymmetric multicomponent formulation. Contrib. Mineral. Petrol. 145, 492–501.
Locock, A.J., 2008. An Excel spreadsheet to recast analyses of garnet into end-member components, and a synopsis of the crystal chemistry of natural silicate garnets. Comput. Geosci. 34, 1769–1780.
Loewy, S.L., Connelly, J.N., Dalziel, I.W.D., 2004. An orphaned basement block: the Arequipa-Antofalla basement of the central Andean margin of South America. Geol. Soc. Am. Bull. 116, 171–187.
Ludwig, K., 2009. Isoplot v. 3.71: A Geochronological Toolkit for Microsoft Excel. Special Publication 4. Berkeley Geochronology Center, Berkeley, California, p. 70.
Martínez, J.C., Dristas, J.A., Massonne, H.-J., 2012. Palaeozoic accretion of the microcontinent Chilenia, North Patagonian Andes: high-pressure metamorphism and subsequent thermal relaxation. Int. Geol. Rev. 54, 472–490.
Massonne, H.-J., Calderón, M., 2008. P–T evolution of metapelites from the Guarguaraz Complex, Argentina: evidence for Devonian) crustal thickening close to the western Gondwana margin. Rev. Geol. Chile 35, 215–231.
Massonne, H.-J., Toulkeridis, Th, 2012. Widespread relics of high-pressure metamorphism confirm major terrane accretion in Ecuador: a new example from the Northern Andes. Int. Geol. Rev. 54, 67–80.
Megard, F., Caldas, J., Paredes, V.J., Cruz, N., 1996. Geología de los cuadrángulos de Tarma, La Oroya y Yauyos (Memoria). INGEMMET, Lima, p. 227. Boletin 69, Serie a.
Mišković, A., Spikings, R.A., Chew, D.M., Košler, J., Ulianov, A., Schaltegger, U., 2009. Tectonomagmatic evolution of Western Amazonia: Geochemical characterization and zircon U–Pb geochronologic constraints from the Peruvian Eastern Cordilleran granitoids. Geol. Soc. Am. Bull. 121, 1298–1324.
Mišković, A., Schaltegger, U., 2009. Crustal growth along a non-collisional cratonic margin: a Lu–Hf isotopic survey of the Eastern Cordilleran granitoids of Peru. Earth Planet. Sci. Lett. 279, 303–315.
Powell, R., Holland, T., 1999. Relating formulations of the thermodynamics of mineral solid solutions: activity modeling of pyroxenes, amphiboles, and micas. Am. Mineral. 84, 1–14.
Ramos, V.A., 2004. Cuyania, an exotic block to Gondwana: review of a historical success and the present problems. Gondwana Res. 7, 1009–1026.
Ramos, V.A., 2008. The basement of the Central Andes: the Arequipa and related terranes. Annu. Rev. Earth Planet. Sci. 36, 289–324.
Ramos, V.A., 2009. Anatomy and global context of the Andes: main geologic features and the Andean orogenic cycle. In: Kay, S.M., Ramos, V.A., Dickinson, W. (Eds.), Backbone of the Americas: Shallow Subduction, Plateau Uplift, and Ridge and Terrane Collision, Geological Society of America Memoir, vol. 204, pp. 31–65.
Ramos, V.A., 2010. The tectonic regime along the Andes: present settings as a key for the Mesozoic regimes. Geol. J. 45, 2–25.
Ramos, V.A., Aleman, A., 2000. Tectonic evolution of the Andes. In: Cordani, U., Milani, E.J., Thomaz Filho, A., Campos Neto, M.C. (Eds.), Tectonic Evolution of South America, International Geolological Congress Rio de Janeiro, pp. 635–685.
Ramos, V.A., Jordan, T.E., Allmendinger, R.W., Mpodozis, C., Kay, S.M., Cortés, J.M., Palma, M.A., 1986. Paleozoic terrains of the central Argentine Chilean Andes. Tectonics 5, 855–880.
Romero, D., Valencia, K., Alarcón, P., Peña, D., Ramos, V.A., 2013. The offshore basement of Perú: evidence for different igneous and metamorphic domains in the forearc. J. South Am. Earth Sci. 42, 47–60.
Sato, K., Tassinari, C.C.G., Kawashita, K., Petronilho, L., 1995. Ométodo geocronológico Sm–Nd no IG/USP e suas aplicações. An. Acad. Bras. Ciências 67, 315–336.
Tassinari, C.C.G., Castroviejo, R., Rodrigues, J.F., Acosta, J., Pereira, E., 2011. A Neoproterozoic age for the chromitite and gabbro of the Tapo ultramafic Massif, Eastern Cordillera, Central Peru and its tectonic implications. J. South Am. Earth Sci. 32, 429–437.
Van Staal, C.R., Whalen, J.B., McNicoll, V.J., Pehrsson, S.J., Lissenberg, C.J., Zagorevski, A., van Breemen, O., Jenner, G.A., 2007. The Notre Dame arc and the Taconic orogeny in Newfoundland. In: Hatcher, R.D., Carlson, M.P., McBride, J.H., Martinez Catalan, J.R. (Eds.), 4-D Framework of Continental Crust, Geological Society of America Memoir, vol. 200, pp. 511–552.
Wakabayashi, J., 1990. Counterclockwise PTt paths from amphibolites, Franciscan Complex, California: relics from the early stages of subduction zone metamorphism. J. Geol. 98, 657–680.
Willner, A.P., Glodny, J., Gerya, T.V., Godoy, E., Massonne, H.-J., 2004. A counterclockwise PTt-path in high pressure-low temperature rocks from the Coastal Cordillera accretionary complex of South Central Chile: constraints for the earliest stage of subduction mass flow. Lithos 73, 283–310.
Willner, A.P., Thomson, S.N., Kröner, A., Wartho, J.A., Wijbrans, J., Hervé, F., 2005. Time markers for the evolution and exhumation history of a late Palaeozoic paired metamorphic belt in central Chile (34°-35°30'S). J. Petrol. 46, 1835–1858.
Willner, A.P., Gerdes, A., Massonne, H.-J., Schmidt, A., Sudo, M., Thomson, S.N., Vujovich, G., 2011. The geodynamics of collision of a microplate (Chilenia) in Devonian times deduced by the pressure–temperature–time evolution within part of a collisional belt (Guarguaraz Complex, W-Argentina). Contrib. Mineral. Petrol. 162, 303–327.
Wilson, J., Reyes, L., 1964. Geología del Cuadrángulo de Pataz. Boletín serie a 9. Instituto Geológico Minero y Metalúrgico, Carta Geológica Nacional, Lima, p. 91. Scale 1:100,000.
Zagorevski, A., van Staal, C.R., 2011. The record of Ordovician arc-arc and arc-continent collisions in the Canadian Appalachians during the closure of Iapetus. In: Brown, D., Ryan, P.D. (Eds.), Arc-Continent Collisions, Frontiers in Earth Sciences. Springer, pp. 344–371.